



Research Article

ISSN : 0975-7384  
CODEN(USA) : JCPRC5

Selective catalytic reduction of NO with NH<sub>3</sub> on stannic and iron bimetal oxides/attapulgite catalysts

Feng Xiao<sup>1</sup>, Yunjie Gu<sup>1</sup>, Zhe Tang<sup>2</sup>, Zhidong Chen<sup>1</sup> and Qi Xu<sup>2\*</sup>

<sup>1</sup>School of Petrochemical Engineering, Changzhou University, Changzhou, Jiangsu Province, China

<sup>2</sup>School of Chemical and Biological Engineering, Yancheng Institute of Technology, Yancheng, Jiangsu Province, China

ABSTRACT

A novel low temperature selective catalytic reduction (SCR) denitration catalyst (1/2SFA) was developed by hydrothermal method in the work and used for NH<sub>3</sub>-SCR reaction. The results show the developed SFA catalyst has excellent catalytic activity for SCR of NO with NH<sub>3</sub>, the NO conversion is up to 96.4% at 200°C. Furthermore, it has good catalyst activity at low temperature (<160°C), wide optimum reaction windows (160-280°C, the NO conversion >90%), and high resisted-poison ability to SO<sub>2</sub>. The catalyst was characterized by Scanning electron microscope (SEM), N<sub>2</sub> adsorption, X-ray diffraction (XRD) and Fourier transform infrared reflectance spectroscopy (FTIR). Besides, the possible reaction mechanism was also involved. It shows that there are existence of interactions between SnO<sub>2</sub> and γ-Fe<sub>2</sub>O<sub>3</sub> on the surface of attapulgite. The γ-Fe<sub>2</sub>O<sub>3</sub> can restrain the growth of SnO<sub>2</sub> crystal. And SnO<sub>2</sub> can improve the dispersions of γ-Fe<sub>2</sub>O<sub>3</sub> particles to form smaller crystal or amorphous particles. In addition, SnO<sub>2</sub> can enhance the ability of catalyst to resist SO<sub>2</sub> poisoning.

**Key words:** Stannic and iron bimetal oxides; attapulgite; selective catalytic reduction; denitration catalysts; hydrothermal method.

INTRODUCTION

Nitrogen oxides (NO<sub>x</sub>) mainly come from coal-fired flue gas and automobile exhaust, which causing photochemical smog, acid rain, ozone depletion and greenhouse effects. Therefore, it is the high time for us to reduce emissions of these harmful compounds. The selective catalytic reduction (SCR) is known as one of the most efficient technologies for eliminating NO<sub>x</sub> from mobile vehicles and stationary power sources [1].

As well known, iron oxide has well NH<sub>3</sub>-SCR NO<sub>x</sub> performance, and remarkable H<sub>2</sub>O durability at high temperature about 300-500°C. Such as, Ma et al. [2] reported the Fe-BEA catalyst prepared by liquid ion exchange method could gain about 100% NO<sub>x</sub> conversion at 350-500°C. Qi et al. [3] reported the Fe/ZSM-5 catalyst shows over 90% NO conversion at range of 350 to 500°C. And after pretreatment in 10% H<sub>2</sub>O at 700°C, the Fe/ZSM-5 still exhibits high activities at temperature higher than 400°C. Others mentioned that Fe-ZSM-5 [4] shown a maximum NO<sub>x</sub> conversion exceeding 90% at 400-550°C in the feed gases with 2% H<sub>2</sub>O.

However, the high-temperature SCR technology requires catalysts have the ability to inherit the toxicity of high sulphur and dust [5]. On the contrary, in the low-temperature SCR technology, the catalyst is located after desulfurizer and dust controller extraction. Hence, it doesn't need high toxicity-resisted ability of sulphur and dust. Moreover, the active metal in low-temperature SCR catalyst can't be easily aggregated together, which causes it has high stability. Thus, the low-temperature SCR technology nowadays gets more and more attention. Many researches were devoted themselves to doing this work and have found that adding additives is one effective way to improve the low-temperature SCR performance of iron-based catalysts. Such as, Cu-Fe/ZSM-5 catalysts [6,7], iron titanate

catalyst [8], Mn-FeO<sub>x</sub>, Fe-Mn/TiO<sub>2</sub>, Fe-Mn/USY catalysts [9-11], Fe-Ce-Mn/ZSM-5, Fe-Ce-Mn/Ti catalysts [12,13].

According to my knowledge, there were no literatures reported Sn-Fe catalysts using in NH<sub>3</sub>-SCR. More important is that many reports demonstrate Sn could improve SCR performance. Zhiming Liu found SnO<sub>2</sub>/Al<sub>2</sub>O<sub>3</sub> catalysts reveal significant performance for selective catalytic reduction of NO<sub>x</sub> with propene [14]. Huazhen Chang found that SnO<sub>2</sub> modified MnO<sub>x</sub>-CeO<sub>2</sub> catalyst can improve the SCR performance and enhance the resistance to SO<sub>2</sub> [15]. Besides, Xiaoliang Li found there was the synergistic effect between SnO<sub>2</sub> and CeO<sub>2</sub> in the Ce<sub>4</sub>Sn<sub>4</sub>O<sub>x</sub> catalyst, which result in the better catalytic performance in a broad temperature range from 100°C to 400°C for NH<sub>3</sub>-SCR [16].

In this work, we used attapulgite (ATP) as support, due to its large surface area, excellent activity and chemical adsorption property and low cost [17,18], to prepare the SFA catalysts, and investigated their catalytic performances for the NO removal during the simulated flue gas in order to discover the effect of Sn in NH<sub>3</sub>-SCR of SFA catalyst. All the samples were characterized by a series of characterization methods, such as Scanning electron microscope (SEM), N<sub>2</sub> adsorption, X-ray diffraction (XRD) and Fourier transform infrared spectrum (FTIR).

## EXPERIMENTAL SECTION

### 1.1 Materials and Chemicals

The raw ATP was provided by Nanjing University Zijin Co. Ltd. (Jiangsu, China). SnCl<sub>4</sub>·4H<sub>2</sub>O, Fe(NO<sub>3</sub>)<sub>3</sub>·9H<sub>2</sub>O, citric acid monohydrate and anhydrous ethanol were purchased from China Chemical Reagent Co. Ltd., and used without further purification.

### 1.2 Synthesis of SFA Catalysts

#### 1.2.1 Preparation of ATP

After calcining at 300°C for 2 h, the raw ATP was treated in 3M acetic acid solutions at 80°C for 4 h under reflux and magnetic string and impregnated for 20 h. Then, it was washed with distilled water to pH = 7 and dried at 105°C overnight. Finally, ATP was obtained after grinding.

#### 1.2.2 Synthesis of SFA catalysts

The SFA catalysts were prepared by conventional hydrothermal method. In the typical process, 3 g of ATP was dispersed in 40mL ethanol solution at ultrasonic dispersion (45 kHz) for 20 min. Afterward, the certain mass of SnCl<sub>4</sub>·4H<sub>2</sub>O, 6mmol Fe(NO<sub>3</sub>)<sub>3</sub>·9H<sub>2</sub>O and 1 g citric acid were added into the solution with stirring until formed sol. The solution was transferred into a Teflon-Lined stainless steel autoclave, sealed, and maintained at 180°C for 12 h, and subsequently cooled in ambient environment to room temperature. The precipitate was filtered, washed with deionized water and absolute ethanol for three times, and dried in vacuum at 60°C for 10 h. The catalysts were gained finally by calcining at 400°C in air in a muffle furnace. The catalysts were denoted as aSFA, where a is the molar of Sn/Fe (a=1/3, 1/2, 2/3), S, F and A are on behalf of SnO<sub>2</sub>, γ-Fe<sub>2</sub>O<sub>3</sub> and ATP, respectively. The SA (SnO<sub>2</sub>/ATP) and FA (Fe<sub>2</sub>O<sub>3</sub>/ATP) are the reference samples prepared with the same method.

### 1.3 Characterization

All the samples were characterized via Scanning electron microscopy (SEM), X-ray diffraction (XRD), FT-IR spectra and N<sub>2</sub> adsorption.

SEM was performed on a scanning electron microscope FEI QUANTA200 operating at 3.00 kV to observe the morphology of the catalysts.

The powder X-ray diffraction datum were collected on a Rigaku D/MAX-2500PC diffractometer operated at 40 kV and 40mA with nickel-filtered Cu Kα radiation (λ = 1.5406 Å). The data was collected in the 2θ range 5-80° with a step size of 0.02° and scan rate of 4° min<sup>-1</sup>.

FT-IR spectra were recorded by a Nicolet 460 spectrometer using the KBr powder technique with diffuse reflectance sampling accessory at a resolution of 4 cm<sup>-1</sup> at room temperature.

N<sub>2</sub> adsorption isotherms of the catalytic materials were measured on an ASAP 2010 Micromeritics. The catalyst surface area and micropore volume were determined from the adsorption branch of the isotherms by applying the BET equation and the t-plot formalism, respectively. Prior to the nitrogen adsorption at -190°C the samples were outgassed at 400°C in vacuum overnight.

### 1.4 NH<sub>3</sub>-SCR Activity Test

The SCR of NO using NH<sub>3</sub> as reductant was carried out between 80°C and 280°C at atmospheric pressure with a quartz tubular down flow reactor (inner diameter 6mm). The catalyst powder (1.25mL, ≈500 mg, particle size < 180 μm) was placed in the reactor. The mixed gases consisting of NO (600ppm), NH<sub>3</sub> (600ppm), O<sub>2</sub> (3 vol. %), 0 or 200ppm SO<sub>2</sub> and N<sub>2</sub> [19], were firstly pre-heated in a gas mixer and then added into the reactor. The content of the outlet gases was online analyzed and monitored by the Flue Gas Analyzer (Vario Plus, German MRU Ltd.). The gas hourly space velocity (GHSV) is 32,000 h<sup>-1</sup> and the NO conversion is calculated as follows [20]:

$$NO_x \text{ conversion}(\%) = \frac{[NO]_{in} - [NO_x]_{out}}{[NO]_{in}} \times 100$$

where NO<sub>x</sub> is the sum of the NO and NO<sub>2</sub> concentrations. The maximum standard deviation of NO<sub>x</sub> conversion and N<sub>2</sub> selectivity are ±1%.

The flow chart of catalyst NH<sub>3</sub>-SCR activity test is shown in the Fig. 1. There are three sections are plenum section (left), reaction section (middle) and analysis section (right), respectively.

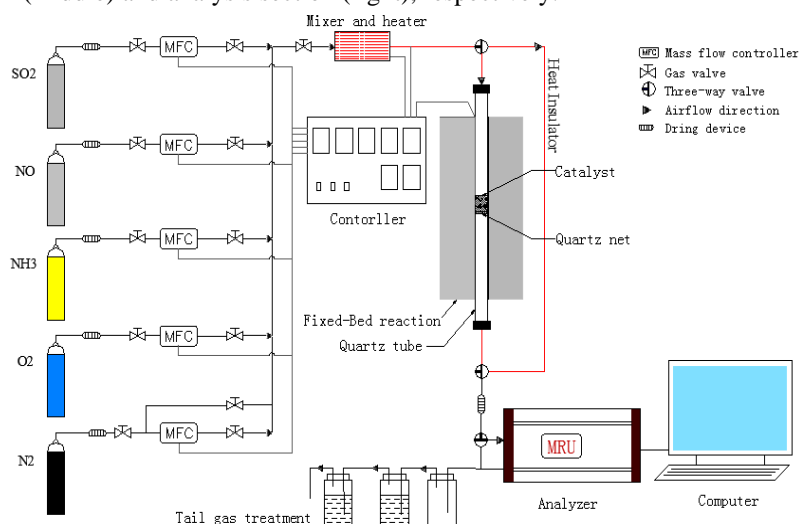


**Fig. 1** the flow chart of catalytic NH<sub>3</sub>-SCR activity test

## RESULTS AND DISCUSSION

### 2.1 Catalyst Characterization

X-ray patterns of all the samples are shown in Fig. 2. The diffraction peaks in Fig. 2a at the 2θ of 8.5°, 13.7°, 19.7° and 27.3° are indexed to the (110), (200), (040), (400) lattice planes of ATP [21], which are in good agreement with the reported ATP results (JCPDS No. 021-0958) [22]. Furthermore, the characteristic reflections for ATP are observed in all of the samples (Figs. 2b-f), which suggests that the structure of ATP is maintained and not destroyed by the modification process. When the iron was introduced into ATP, the characteristic diffraction peaks of γ-Fe<sub>2</sub>O<sub>3</sub> appeared at 2θ=30.53°, 35.48°, 57.34°, 63.02°, indexed to the (220), (331), (233), (440) lattice planes of γ-Fe<sub>2</sub>O<sub>3</sub> (Fig. 2b). The result indicates γ-Fe<sub>2</sub>O<sub>3</sub> is formed in FA (Fe<sub>2</sub>O<sub>3</sub>/ATP). Further impregnating tin into FA (Figs. 2c-e) or ATP (Fig. 2f), the characteristic diffraction peaks of SnO<sub>2</sub> at 2θ=26.57° (110), 33.86° (101), 51.77° (211) were observed, which demonstrates the formation of SnO<sub>2</sub>. Carefully observing, it was found with the increasing amounts of SnO<sub>2</sub>, the characteristic reflection peaks of γ-Fe<sub>2</sub>O<sub>3</sub> will become weaker and weaker (Figs. 2c-d) until nearly disappear in 2/3 SFA (Fig. 2e). While the peaks of SnO<sub>2</sub> in SFA catalysts don't change largely, only has slight increased. However, when there is no γ-Fe<sub>2</sub>O<sub>3</sub> (SA, Fig. 2f), the diffraction peaks of SnO<sub>2</sub> are changed significantly both in intensity and width. Its intensity increase large and its width become very narrow. The results indicate that there are existence of some interactions between Sn (SnO<sub>2</sub>) and Fe (γ-Fe<sub>2</sub>O<sub>3</sub>). The γ-Fe<sub>2</sub>O<sub>3</sub> can retard the growth of SnO<sub>2</sub> crystal. And SnO<sub>2</sub> can improve the dispersions of γ-Fe<sub>2</sub>O<sub>3</sub> particles to form smaller crystal or amorphous particles [23], which would be in favor of NH<sub>3</sub>-SCR to NO.

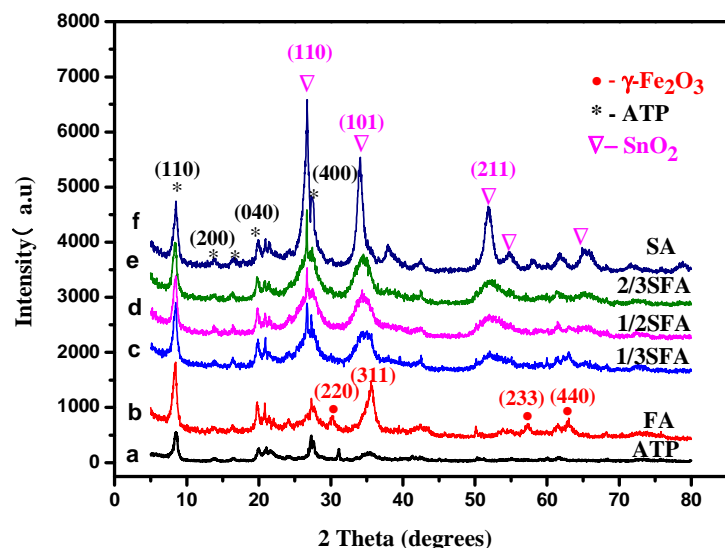
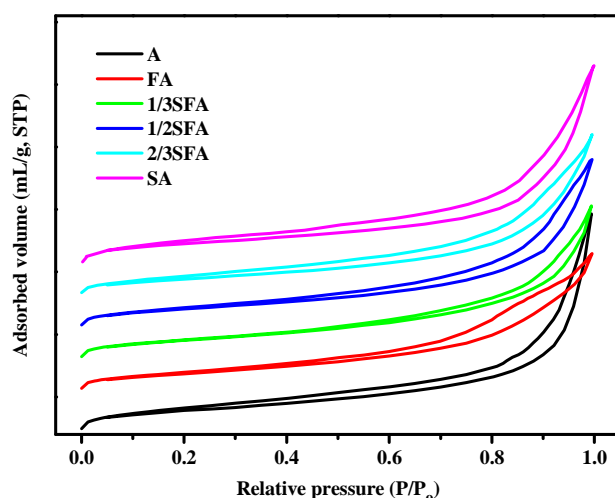


Fig. 2 the XRD patterns of all the samples

Their porous structures were investigated by  $N_2$  adsorption and desorption measurement. Fig.3 is their  $N_2$  adsorption-desorption isotherms diagram, which shows that all the samples are characteristic of type IV isotherms with type  $H_3$  hysteresis loops, indicating the formation of mesoporous [24]. Fig.4 is their typical BJH pore size distribution patterns. It can be seen that mesoporous exist in all the samples. ATP (A) has hierarchically organized porous size distributions with two small narrow pore sizes at 1.81 and 4.06 nm and two large shoulder pore sizes centered at 15.94 and 27.04 nm. After impregnation of  $\gamma\text{-Fe}_2\text{O}_3$  into ATP (FA), the large shoulder pore sizes disappear, and many new small pore sizes between 1.80 and 20.50 nm appear. Further introduction of  $\text{SnO}_2$  into FA (SFA), these small pore sizes become more concentration and uniform with increasing molar amount of  $\text{SnO}_2$ . When the molar ratio of Sn/Fe is up to 1/2, the small pore sizes (1/2SFA) are centralized at 3.78 nm. Namely, there is only one small pore size between 2.0 to 14.0 nm centered at 3.78 nm. However, further increase of the molar ratio of Sn/Fe into 2/3 (2/3SFA), several weak shoulder pore sizes centered at 10.53, 16.20 and 22.65 nm appear beside the small pore size at 3.78 nm. When there is only  $\text{SnO}_2$  in the ATP (SA), beside the shoulder peak at 10.53 nm and small pore size at 3.78 nm, several other weak pore sizes appear, such as 8.61, 5.51 and 2.21 nm. Together with the results of XRD, they indicated that after impregnation of  $\gamma\text{-Fe}_2\text{O}_3$  into ATP (FA), the  $\gamma\text{-Fe}_2\text{O}_3$  crystals were formed in the surface of ATP and covered or blocked pore structure of ATP and formed some new pore structures by themselves. Because  $\text{SnO}_2$  can improve the dispersions of  $\gamma\text{-Fe}_2\text{O}_3$  particles, when continually introduced  $\text{SnO}_2$  into FA, the pore size was becoming more concentration and uniform until the molar ratio of Sn/Fe was up to 1/2. Although  $\gamma\text{-Fe}_2\text{O}_3$  can retard the growth of  $\text{SnO}_2$ , after the molar ratio of Sn/Fe got to 2/3, the  $\text{SnO}_2$  crystal had a certain degree of growth and formed some very weak peaks by themselves. When there is only  $\text{SnO}_2$  on ATP,  $\text{SnO}_2$  crystal grown up quickly without retardation of  $\gamma\text{-Fe}_2\text{O}_3$  and several other pores appear.

Fig. 3 the  $N_2$  sorption-desorption isotherms of all the samples

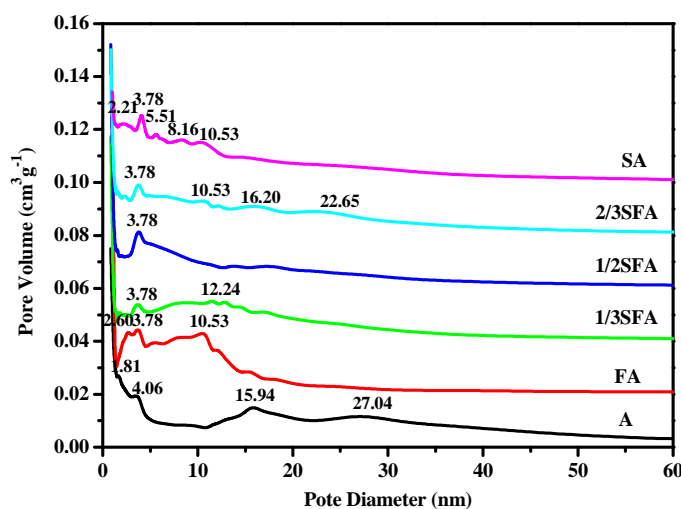


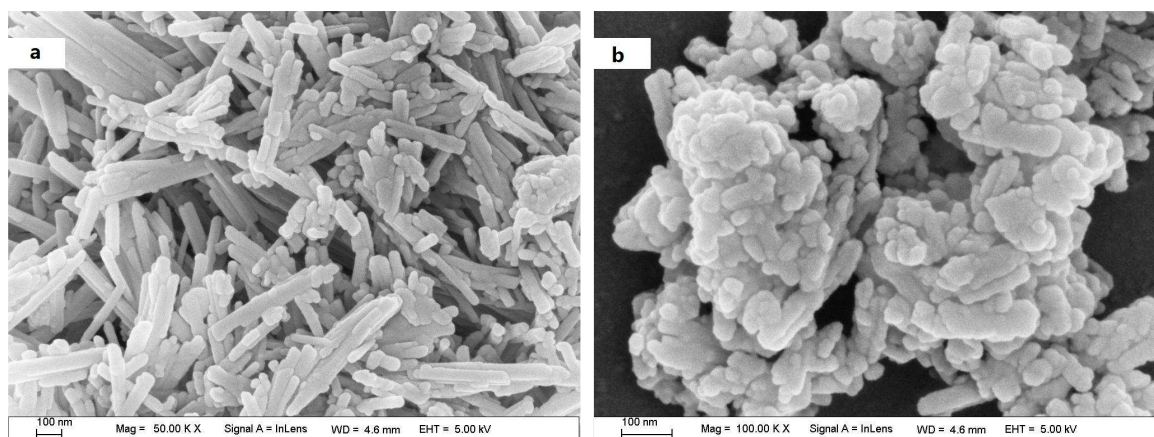
Fig. 4 the pore diameter distribution patterns of all the samples

The presumption is confirmed by the textural properties in Table 1 and SEM in Fig. 5. In Table 1, due to coverage and blocking of  $\gamma\text{-Fe}_2\text{O}_3$ , the BET special surface area and pore volume are decreased significantly from  $171.0\text{ m}^2\text{ g}^{-1}$ ,  $0.55\text{ cm}^3/\text{g}$  (ATP) to  $133.1\text{ m}^2\text{ g}^{-1}$  and  $0.36\text{ cm}^3/\text{g}$  (FA) respectively, after impregnation of  $\gamma\text{-Fe}_2\text{O}_3$  into ATP. Because of the dispersions of  $\text{SnO}_2$  to  $\gamma\text{-Fe}_2\text{O}_3$ , the  $\gamma\text{-Fe}_2\text{O}_3$  crystal or particles become more small and uniform. The BET special surface area and pore volume should be increased gradually, like the results in Table 1.

Table 1 BET surface area and pore structure results of all the samples

Catalyst	Surface Area $\text{m}^2/\text{g}$	Pore Volume $\text{cm}^3/\text{g}$	Pore Diameter $D_v(\text{d})\text{ nm}$
ATP	171.0	0.55	13.44
FA	133.1	0.36	10.68
1/3SFA	127.6	0.41	12.99
1/2SFA	138.7	0.42	11.72
2/3SFA	144.4	0.43	10.96
SA	165.3	0.45	9.58

More detail observation can be seen in SEM. Four typical samples are checked by SEM (shown in Fig.5). It can be seen in Fig. 5a that ATP is a uniform stick structure with smooth surface, which is favorable for adhesion between the coating and the substrate. But after impregnation of  $\gamma\text{-Fe}_2\text{O}_3$  into ATP (FA), the ATP stick structure is hardly to observe, many big irregular particles ( $\gamma\text{-Fe}_2\text{O}_3$ ) appear on the surface of ATP (Fig.5b), and the irregular particles ( $\gamma\text{-Fe}_2\text{O}_3$ ) aggregate together, which may cause the BET special surface and pore volume decrease enormously and form some new pores by the aggregated particles ( $\gamma\text{-Fe}_2\text{O}_3$ ). However, after a certain amount of  $\text{SnO}_2$  is introduced into FA (1/2SFA), the aggregated particles disappear, ATP stick structure is clearly observed, and the loaded metal oxides are uniformly dispersed on the surfaces of ATP (Fig.5c), which are consistent with the results of BET (the BET special surface and pore volume increase and pore sizes get more uniform). When there is only  $\text{SnO}_2$  on the surface of ATP (SA, Fig.5d), there appear many small irregular particles on or around the surface of ATP, resulting in formation of some new pores by the small irregular particles.



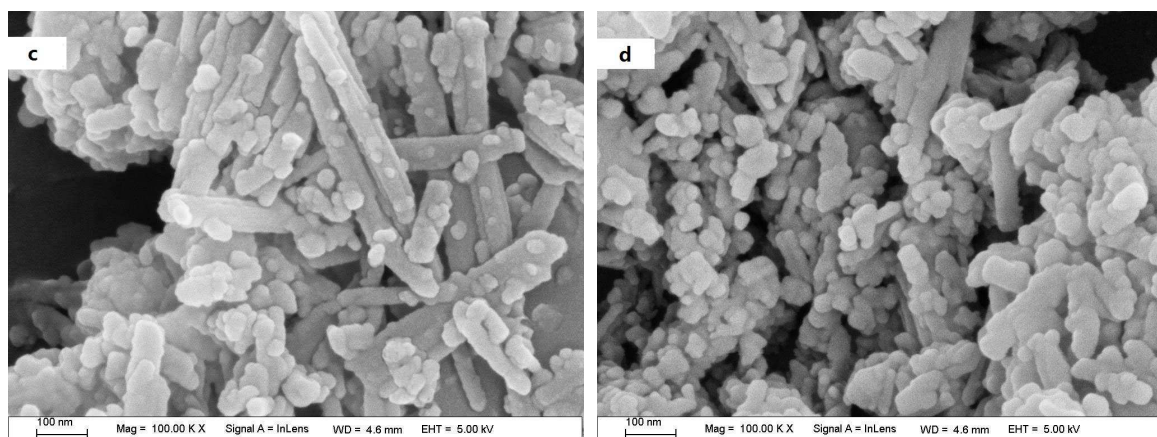


Fig. 5 the SEM images of four the samples, (a) ATP, (b) FA, (c) 1/2SFA and (d) SA

## 2.2. Catalytic Activity

### 2.2.1. The $\text{NH}_3$ -SCR Activity

The NO conversions over various catalysts with different Sn/Fe molar ratios are shown in Fig.6. The results indicate that the Sn/Fe molar ratio has a great influence on the NO conversion. FA ( $\gamma\text{-Fe}_2\text{O}_3$ /ATP) catalyst has good activity at 200°C with 95.7% NO conversion. However, it has very narrow reaction window. Once the reaction temperature is high or below than 200°C, the catalytic activity (NO conversion) decreases quickly, especially at low temperature. The result indicates that the individual active metal  $\gamma\text{-Fe}_2\text{O}_3$  on ATP has poor catalytic stability of  $\text{NH}_3$ -SCR to NO, especially at low temperature. However, when  $\text{SnO}_2$  is introduced into FA, the phenomena have changed. The SFA catalyst has wide optimum reactive active window and higher catalyst activity at low temperature (<160°C). The 1/3 SFA has optimum SCR activity between 160 and 240°C with highest NO conversion (94.3%) closed to that of FA, and has better catalyst activity at other temperature (< 160°C or >240°C). The result indicates  $\text{SnO}_2$  can activate the low temperature SCR activity of  $\gamma\text{-Fe}_2\text{O}_3$  and stabilize the optimum SCR activity. When the molar ratio of Sn/Fe increases to 1/2, the SCR performance of catalyst is sequentially enhanced. The 1/2 SFA has superior SCR activity in the whole reaction temperature realm in all the catalysts. The reaction activity window is enlarged into 160 to 280°C, and the optimum NO conversion of 1/2SFA is higher than that of FA, up to 96.4 % at temperature range of 200 to 240°C. However, further increasing the molar ratio of Sn/Fe up to 2/3, the phenomena have changed. Although the catalyst (2/3SFA or SA) has large reaction windows, the catalyst activity is declined significantly. The optimum NO conversion is just only 79.8 % (quite lower than 95.7% NO conversion of FA). Its catalyst activity is similar to that of SA ( $\text{SnO}_2$ /ATP), indicating that most of the main active metal  $\gamma\text{-Fe}_2\text{O}_3$  is more possibly covered by the auxiliary reagent  $\text{SnO}_2$ . The results are agreement with the results of XRD and BET. When the molar ratio of Sn/Fe is below 1/2,  $\text{SnO}_2$  is improving dispersion of  $\gamma\text{-Fe}_2\text{O}_3$  on the catalyst to form smaller  $\gamma\text{-Fe}_2\text{O}_3$  particles and itself is not so big to cover the active metal  $\gamma\text{-Fe}_2\text{O}_3$  (The  $\gamma\text{-Fe}_2\text{O}_3$  diffraction peaks can be found in XRD patterns of 1/2SFA in Fig.2 and there is no big pore size shoulder peak formed by  $\text{SnO}_2$  in Fig.4). Since the total molar amount of exposed  $\gamma\text{-Fe}_2\text{O}_3$  on the catalyst is constant, smaller  $\gamma\text{-Fe}_2\text{O}_3$  is, stronger the catalyst activity is, lower the reaction energy barrier is. Hence, it has higher activity at low temperature (< 160°C). Moreover, the interaction of  $\text{SnO}_2$  and  $\gamma\text{-Fe}_2\text{O}_3$  inhibits the aggregation of  $\gamma\text{-Fe}_2\text{O}_3$  particles and stabilizes the catalyst activity. However, when the molar ratio of Sn/Fe is up to 2/3,  $\text{SnO}_2$  will be possible to cover the so small active metal  $\gamma\text{-Fe}_2\text{O}_3$  (it is hard to find  $\gamma\text{-Fe}_2\text{O}_3$  diffraction peaks in XRD patterns of Fig.2 and some larger shoulder peaks formed by  $\text{SnO}_2$  appear in Fig.4), leading the catalyst activity of 2/3SFA is similar to that of SA ( $\text{SnO}_2$ /ATP).

In order to further investigate and understand the interaction between  $\text{SnO}_2$  and  $\gamma\text{-Fe}_2\text{O}_3$ , three FT-IR experiments,  $\gamma\text{-Fe}_2\text{O}_3$  (FA without ATP),  $\text{SnO}_2$ (SA without ATP) and  $\gamma\text{-Fe}_2\text{O}_3$ / $\text{SnO}_2$  (1/2SFA without ATP), were carried out. The result is shown in Fig.7. It can be seen that all the samples appear the absorption peaks at 3421 and 1630  $\text{cm}^{-1}$ , which are attributed to the stretching vibrations of OH groups in the hydroxide structure as well as physically adsorbed water. Since the three samples are prepared and calcined in the same conditions, the intensities or areas of the bands are connected with the special surface area. Larger special surface area is, easier the water is to adsorb on the catalyst, stronger the bands is [25]. From the above results,  $\text{SnO}_2$  can improve the dispersion of  $\gamma\text{-Fe}_2\text{O}_3$  on ATP. Hence, the intensities of the bands at  $\gamma\text{-Fe}_2\text{O}_3$ / $\text{SnO}_2$  are larger than that of  $\gamma\text{-Fe}_2\text{O}_3$ . The characteristic peaks of  $\gamma\text{-Fe}_2\text{O}_3$  and  $\text{SnO}_2$  appear in the fingerprint region at 400-1100  $\text{cm}^{-1}$  (the inset picture in Fig. 7). For  $\gamma\text{-Fe}_2\text{O}_3$ , the bands at 538 and 466  $\text{cm}^{-1}$  are due to the stretching vibration of Fe-O [26]. The characteristic IR spectra of  $\text{SnO}_2$  appear at 619 and 1041  $\text{cm}^{-1}$  [27, 28]. However, in the  $\gamma\text{-Fe}_2\text{O}_3$ / $\text{SnO}_2$ , the conditions changed. The characteristic peaks of  $\gamma\text{-Fe}_2\text{O}_3$  get blue shift from 538, 466  $\text{cm}^{-1}$  to 542, 473  $\text{cm}^{-1}$ , respectively. While, the characteristic peak of  $\text{SnO}_2$  at 619  $\text{cm}^{-1}$  has red shifted to 581  $\text{cm}^{-1}$ . In addition, all the characteristic peaks became very weak and board. These results demonstrate that there are interactions between  $\text{SnO}_2$  and  $\gamma\text{-Fe}_2\text{O}_3$  [29, 30], which can confirm the

hypotheses from the XRD, SEM and BET conclusion. However, the detail interaction mechanism of SnO<sub>2</sub> and  $\gamma$ -Fe<sub>2</sub>O<sub>3</sub> is not understood now, many works are underway.

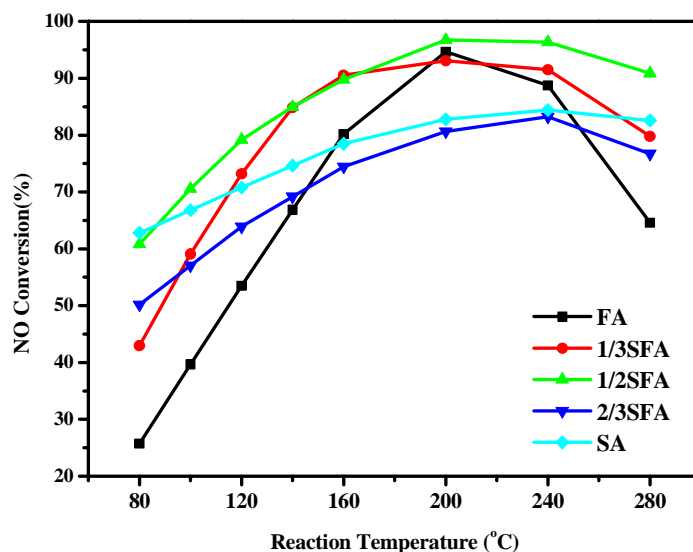


Fig. 6 the NO conversions of all the catalysts

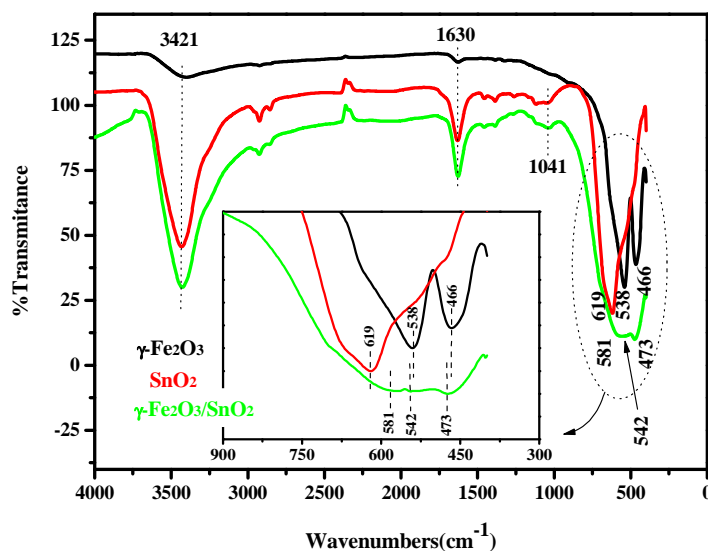


Fig. 7 the FTIR spectra of FA, SA and SFA without ATP

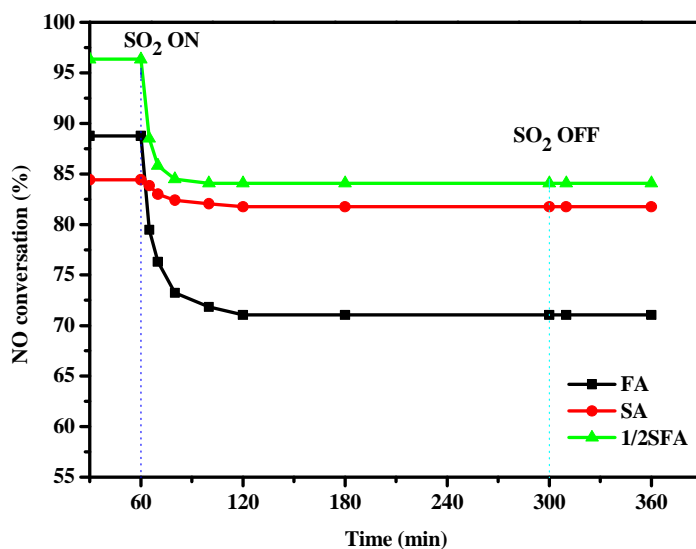


Fig. 8 the SO<sub>2</sub> tolerance of FA, SA and 1/2SFA

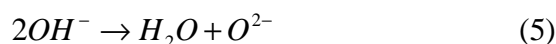
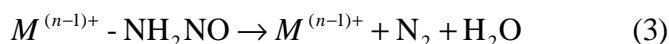
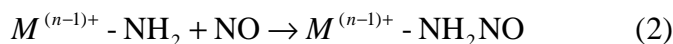
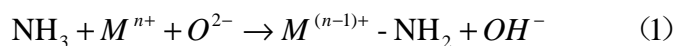
### 2.2.2. Effect of SO<sub>2</sub> on SCR Activity

In order to further understand the effect of reaction condition (SO<sub>2</sub>) and SnO<sub>2</sub> on activity of the catalyst. Two kinds of SO<sub>2</sub> concentration (0ppm and 200ppm) are designed in the work and the corresponding results (NO conversion) are shown in Fig.8. It can be seen that in the absence of SO<sub>2</sub> the catalyst activity is as follows: 1/2SFA>FA>SA, the same with the above result. But after introduction of SO<sub>2</sub> into the reaction system, the catalyst activity is quickly declined and then stabilized at certain level. The declined degree of catalyst activity is as follows: FA>1/2SFA>SA, the final stable catalyst activity in presence of SO<sub>2</sub> atmosphere is 1/2SFA>SA>FA. The results suggest that SO<sub>2</sub> can poison partly the 1/2SFA catalyst activity of NH<sub>3</sub>-SCR. This is an advantage of the low temperature of SCR technology in industry, whose catalyst is played after dust and sulfur extraction. In addition, the results show that SnO<sub>2</sub> has high sulfur tolerance ability compared with γ-Fe<sub>2</sub>O<sub>3</sub>.

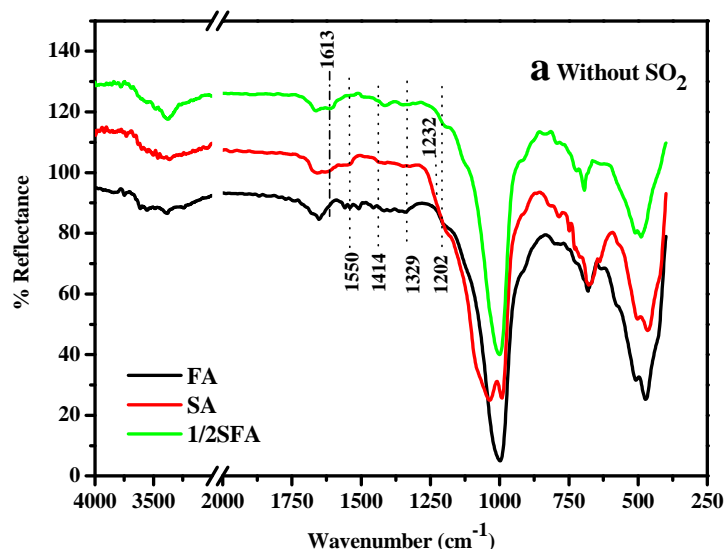
### 2.3. FTIR Analysis

In order to investigate the mechanism of well sulfur tolerance of SnO<sub>2</sub>, the FTIR studies were carried out in our experiment with the spent catalysts, which were exposed in catalytic reaction gases with SO<sub>2</sub> or not at 200°C for 60 minutes, respectively, and the FTIR spectra are shown in Fig.9 (a: without SO<sub>2</sub>, b: with SO<sub>2</sub>). The feed reaction gases contains 600ppm NO, 600ppm NH<sub>3</sub>, 3 vol. % O<sub>2</sub>, 0 or 200ppm SO<sub>2</sub> and balanced gas N<sub>2</sub>.

In Fig.9a, the obvious and strong adsorption peaks are attributed to vibration adsorption peaks of physically adsorbed water or supporter ATP (3417, 1656, 1000, 680 and 500 cm<sup>-1</sup>) [24, 31, 32]. However, there is still existence of some weak peaks at range of 1230-1660 cm<sup>-1</sup>, which are attributed to vibration of adsorbed nitrogen species, such as nitrite (1232 cm<sup>-1</sup>) and monodentate (1550 cm<sup>-1</sup>), bidentate (1329 cm<sup>-1</sup>) and bridge nitrate (1613 cm<sup>-1</sup>) [33-36]. Besides, the band at 1202 cm<sup>-1</sup> is ascribed to coordinated NH<sub>3</sub> on Lewis acid sites [33, 34, 37], but the band at 1414 cm<sup>-1</sup> assigned to the free of NH<sub>4</sub><sup>+</sup> on Brønsted acid sites [34] was not obviously. The results indicate that the mechanism of our NH<sub>3</sub>-SCR of NO reaction is similar with the NH<sub>2</sub>-NO mechanism [38, 39]. Firstly, NH<sub>3</sub> is adsorbed in the Lewis acid sites. Along with reduction of catalyst, the NH<sub>3</sub> is activated into -NH<sub>2</sub> (Eq. (1)). Then, the activation of -NH<sub>2</sub> interacts with NO to formation of intermediate nitrosamine (Eq. (2)). Finally, intermediate nitrosamine decomposes into N<sub>2</sub> and H<sub>2</sub>O (Eq. (3)) as well as oxidation of catalyst (Eq. (4)) and condensation of OH<sup>-</sup> (Eq. (5)). The possible reaction mechanism is shown in Sch. 1.



Sch. 1 Possible reaction mechanism of NH<sub>3</sub>-SCR of NO



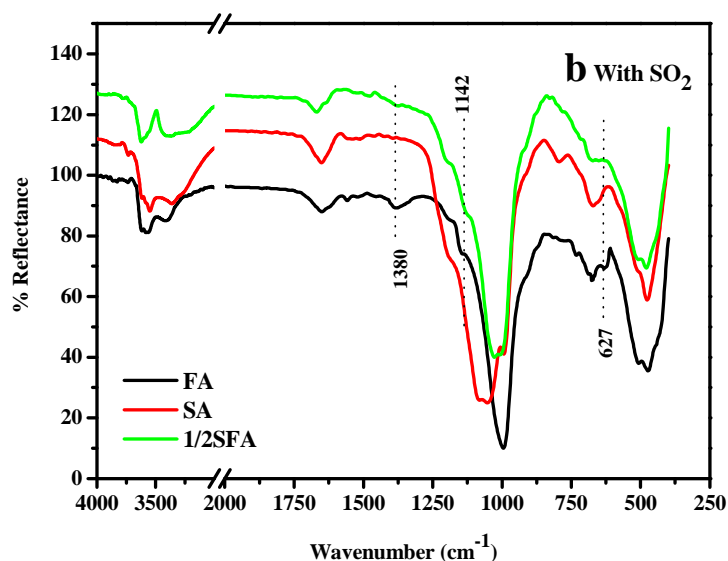


Fig. 9 the FTIR spectra of spent catalysts (a) in presence of SO<sub>2</sub> or not (b)

Fig.9b is the FT-IR spectra of the spent catalyst under SO<sub>2</sub>. Similarly with the Fig. 9a, most of the obvious and strong adsorption peaks are attributed to vibration adsorption peaks of supporter ATP or physically adsorbed water. However, suffered from SO<sub>2</sub> poison, it emerges some new absorption peaks on the spent catalysts. The band at 1380 cm<sup>-1</sup> is attributed to asymmetric vibration mode of O=S=O, which is typical organic sulfate species with covalent S=O double bonds [40]. The bands at 1142 and 627 cm<sup>-1</sup> are attributed to the free inorganic SO<sub>4</sub><sup>2-</sup> [41], which implies the formation of ammonium sulfate, which may be reason of SO<sub>2</sub> poison to catalyst. The formation of ammonium sulfate will be possible to block the pore size and occupy or cover the active site leading the NH<sub>3</sub>-SCR activity of catalyst decrease. For the FA catalyst these absorption peaks (1380, 1142 and 627 cm<sup>-1</sup>) can be clearly observed. But they are not clear on SA and 1/2SFA. The results indicate that SnO<sub>2</sub> can inhibit the reaction of NH<sub>3</sub> and SO<sub>2</sub> to formation of (NH<sub>4</sub>)<sub>2</sub>SO<sub>4</sub> to decrease the poison of SO<sub>2</sub>.

## CONCLUSION

A novel low temperature SCR catalyst (1/2SFA) is developed in the work and used to NH<sub>3</sub>-SCR NO reaction. The results show the developed SFA catalyst has excellent catalytic activity for SCR of NO with NH<sub>3</sub>, the best NO conversion is up to 96.4 % at 200°C. Furthermore, it also has good catalyst activity at low temperature (<160°C), wide optimum reaction windows (160-280°C), and high resisted-poison ability to SO<sub>2</sub>. The possible reaction mechanism is involved in the work. It shows that there are some interactions between SnO<sub>2</sub> and γ-Fe<sub>2</sub>O<sub>3</sub> of the catalyst. The γ-Fe<sub>2</sub>O<sub>3</sub> can restrain the growth of SnO<sub>2</sub> crystal. SnO<sub>2</sub> can improve the dispersions of γ-Fe<sub>2</sub>O<sub>3</sub> particles to form smaller crystal or amorphous particles. Besides, SnO<sub>2</sub> can enhance the ability of catalyst to resist SO<sub>2</sub> poisoning.

## Acknowledgements

This work was supported financially by the Innovation Fund Project of Yancheng Institute of Technology (YKB201106) and the Open Fund Project of Environmental Protection Department of Jiangsu Province (2012019).

## REFERENCES

- [1] F Liu; H He. *J. Phys. Chem. C.*, **2010**, 114(40), 16929-16936.
- [2] L Ma; H Chang; S Yang; L Chen; L Fu; J Li. *Chem. Eng. J.*, **2012**, 209, 652-660.
- [3] G Qi; Y Wang; R Yang. *Catal. Lett.*, **2008**, 121(1-2), 111-117.
- [4] P Metkar; M Harold; V Balakotaiah. *Appl. Catal. B-Environ.*, **2012**, 111-112(0), 67-80.
- [5] M Klimczak; P Kern; T Heinzelmann; M Lucas; P Claus. *Appl. Catal. B-Environ.*, **2012**, 111-112(0), 67-80.
- [6] A Sultana; M Sasaki; K Suzuki; H Hamada. *Catal. Commun.*, **2013**, 41, 21-25.
- [7] S Brandenberger; O Kröcher; A Tissler; R Althoff. *Ind. Eng. Chem. Res.*, **2011**, 50(8), 4308-4319.
- [8] F Liu; H He; C Zhang; Z Feng; L Zheng; Y Xie; T Hu. *Appl. Catal. B-Environ.*, **2010**, 96(3-4), 408-420.
- [9] S Yang; C Wang; J Li; N Yan; L Ma; H Chang. *Appl. Catal. B-Environ.*, **2011**, 110, 71-80.
- [10] Z Wu; B Jiang; Y Liu. *Appl. Catal. B-Environ.*, **2008**, 79(4), 347-355.
- [11] Q Lin; J Li; L Ma; J. Hao. *Catal. Today*, **2010**, 151(3-4), 251-256.
- [12] G Zhou; B Zhong; W Wang; X Guan; B Huang; D Ye; H Wu. *Catal. Today*, **2011**, 175(1), 157-163.

- [13] B Shen; T Liu; N Zhao; X Yang; L Deng. *J. Environ. Sci.*, **2010**, 22(9), 1447-1454.
- [14] Z Liu; J Li; J Hao. *Chem. Eng. J.*, **2010**, 165(2), 420-425.
- [15] H Chang; J Li; X Chen; L Ma; S Yang; J Schwank; J. Hao. *Catal. Commun.*, **2012**, 27(1), 54-57.
- [16] X Li; Y Li; S Deng; T Rong. *Catal. Commun.*, **2013**, 40, 47-50.
- [17] Y Deng; Z Gao; B Liu; X Hu; Z Wei; C Sun. *Chem. Eng. J.*, **2013**, 223(0), 91-98.
- [18] Q Fan; X Tan; J Li; X Wang; W Wu; G Montavon. *Environ. Sci. Technol.*, **2009**, 43(15), 5776-5782.
- [19] B Shen; Y Wang; F Wang; T Liu. *Chem. Eng. J.*, **2014**, 236(0), 171-180.
- [20] H Xu; Y Wang; Y Cao; Z Fang; T Lin; M Gong; Y Chen. *Chem. Eng. J.*, **2014**, 240(0), 62-73.
- [21] J Cao; G Shao; Y Wang; Y Liu; Z Yuan. *Catal. Commun.*, **2008**, 9(15), 2555-2559.
- [22] X Li; X Lu; Y Meng; C Yao; Z. Chen. *J. Alloy. Compd.*, **2013**, 562(0), 56-63.
- [23] H Chang; J Li; J Yuan; L Chen; Y Dai; H Arandiyani; J Xu; J Hao. *Catal. Today*, **2013**, 201, 139-144.
- [24] X Zhao; Y Meng; X Lu; X Li. *J. Sol-Gel Sci. Technol.*, **2013**, 66(1), 22-30.
- [25] S Deng; H Li; Y Zhang. *Chinese J. Inorg. Chem.*, **2003**, 19(08), 825-830.
- [26] Z Jing. *Mater. Lett.*, **2006**, 60 (17-18), 2217-2221.
- [27] D Amalric-Popescu; F Bozon-Verduraz. *Catal. Today*, **2001**, 70(1-3), 139-154.
- [28] Y Zeng; Z Liu; H Liu. *Chinese J. Catal.*, **2008**, 29(03), 253-258.
- [29] W Wang; D Li; Z Wang; H Cui; G Xue. *Chinese J. Inorg. Chem.*, **2002**, 18(08), 823-826.
- [30] B Zhang; Y Tian; J Zhang; W Cai. *Mater. Lett.*, **2011**, 65(8), 1204-1206.
- [31] L Bouna; B Rhouta; M Amjoud; F Maury; M Lafont; A Jada; F Senocq; L Daoudi. *Appl. Clay. Sci.*, **2011**, 52(3), 301-311.
- [32] L Zhang; F Lv; W Zhang; R Li; H Zhong; Y Zhao; Y Zhang; X Wang. *J. Hazard Mater.*, **2011**, 52 (3), 301-311.
- [33] Y Shi; S Chen; H Sun; Y Shu; X Quan. *Catal. Commun.*, **2013**, 42, 10-13.
- [34] J Yu; F Guo; Y Wang; J Zhu; Y Liu; F Shu; S Gao; G Xu. *Appl. Catal. B-Environ.*, **2010**, 95(1-2), 160-168.
- [35] J Li; Y Zhu; R Ke; J Hao. *Appl. Catal. B-Environ.*, **2008**, 80(3-4), 202-213.
- [36] H He; J Wang; Q Feng; Y Yu; K Yoshida. *Appl. Catal. B-Environ.*, **2003**, 46(2), 365-370.
- [37] B Jiang; Z Li; S Lee. *Chem. Eng. J.*, **2013**, 225, 52-58.
- [38] G Ramis; G Busca; F Bregani; P Forzatti. *Appl. Catal.*, **1990**, 64(0), 259-278.
- [39] P Forzatti. *Appl. Catal. A-Gen.*, **2001**, 222(1-2), 221-236.
- [40] F Liu; K Asakura; H He; W Shan; X Shi; C Zhang. *Appl. Catal. B-Environ.*, **2001**, 222(1-2), 221-236.
- [41] S Yang; Y Guo; H Chang; L Ma; Y Peng; Z Qu; N Yan; C Wang; J Li. *Appl. Catal. B-Environ.*, **2013**, 136-137, 19-28.